

HandSplat: Embedding-Driven Gaussian Splatting for High-Fidelity Hand Rendering

Yilan Dong¹ Haohe Liu² Qing Wang¹ Jiahao Yang¹ Wenqing Wang²

Gregory Slabaugh¹ Shanxin Yuan¹

¹Queen Mary University of London ²University of Surrey

{yilan.dong, qing.wang, jiahao.yang, g.slabaugh, shanxin.yuan}@qmul.ac.uk

{haohe.liu, wenqing.wang}@surrey.ac.uk

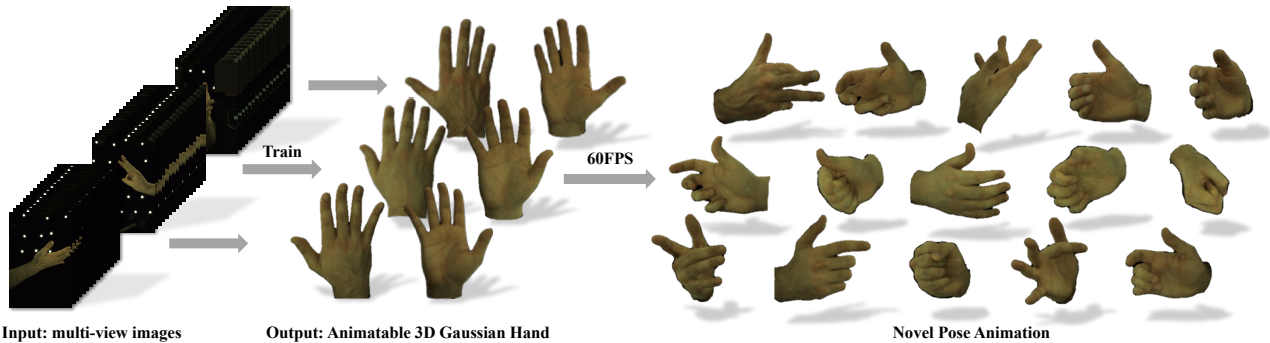


Figure 1. We introduce **HandSplat**, an efficient method for creating an animatable 3D Gaussian hand. Given a set of hand images with skeleton poses and foreground masks, our approach reconstructs a high-fidelity 3D Gaussian hand that enables real-time novel pose animation at over 60 FPS, achieving superior rendering quality compared to state-of-the-art methods [2, 8, 20].

Abstract

Existing 3D Gaussian Splatting (3DGS) methods for hand rendering rely on rigid skeletal motion with an oversimplified non-rigid motion model, which fails to capture fine geometric and appearance details. Additionally, they perform densification based solely on per-point gradients and process poses independently, ignoring spatial and temporal correlations. These limitations lead to geometric detail loss, temporal instability, and inefficient point distribution. To address these issues, we propose **HandSplat**, a novel Gaussian Splatting-based framework that enhances both fidelity and stability for hand rendering. To improve fidelity, we extend standard 3DGS attributes with implicit geometry and appearance embeddings for finer non-rigid motion modeling while preserving the static hand characteristic modeled by original 3DGS attributes. Additionally, we introduce a local gradient-aware densification strategy that dynamically refines Gaussian density in high-variation regions. To improve stability, we incorporate pose-conditioned attribute regularization to encourage attribute consistency across similar poses, mitigating temporal artifacts. Extensive experiments on InterHand2.6M demonstrate that HandSplat surpasses existing methods in fidelity and stability while achieving real-time performance. We will release the code and pre-trained models upon ac-

ceptance.

1. Introduction

Rendering photorealistic hands is a challenging yet essential problem for applications such as augmented and virtual reality (AR/VR), immersive gaming, and human-computer interaction. As a key interface for interaction, hands play a crucial role in digital environments, making their realism essential for immersion and usability. To achieve life-like rendering, it's crucial to capture both intricate motion and fine-grained appearance while ensuring real-time performance, high visual fidelity and stability.

Recent advancements in 3D Gaussian Splatting (3DGS) [13] have enabled efficient, high-quality rendering by modeling deformable targets with continuous and differentiable Gaussian primitives. Unlike NeRF-based [18] methods [4, 6, 7], which suffer from slow inference due to dense ray sampling and multilayer perceptron (MLP) computations, 3DGS offers real-time rendering capability while preserving high visual quality. Leveraging these advantages, 3DGS has been extended to articulated human bodies and hands [8, 11, 22, 24, 27, 30], where representations are initialized in a canonical space and deformed into the posed space through rigid skeletal motion.

Despite recent progress, 3DGS-based methods [8, 11, 22, 24, 27, 30] still suffer from fundamental limitations in both fidelity and stability for hand rendering. First, they exhibit limited fidelity in non-rigid modeling (e.g., knuckle protrusions, skin stretching, and shadow variations) due to their reliance on simplistic MLP architectures, which fail to capture high-frequency details. While increasing network capacity could improve accuracy, it incurs high computational costs, compromising 3DGS’s efficiency. Moreover, original attributes in 3DGS inherently tend to represent the static geometry and appearance of the hand. Incorporating these attributes into the optimization of motion-related variations can interfere with their static representation, leading to inaccurate parameter updates. Second, the densification strategies designed for static-scene 3DGS [11, 13, 24] are inadequate for dynamic hands, further limiting fidelity. These strategies rely solely on per-point gradients for splitting and merging, restricting the adaptive refinement of point density in high-detail regions. Consequently, areas with complex structure, such as emerging palm creases during fist closure, may lack sufficient density to capture fine details. Third, existing methods [8, 15, 27, 30] process each hand pose independently, overlooking the fact that similar hand poses often share consistent Gaussian attributes. They neither leverage this intrinsic correlation nor transfer learned attributes across frames, potentially leading to unstable or suboptimal rendering by failing to reference better-optimized Gaussian attributes from similar poses. These limitations collectively hinder the fidelity and stability of 3D hand rendering, particularly under complex articulations and lighting conditions.

To address these challenges, we propose HandSplat, a fast Gaussian Splatting-based method that enables hand rendering with improved fidelity and stability. First, we extend standard 3DGS with two implicit attributes: geometry and appearance embeddings to capture the motion-related local hand characteristics. This approach prevents the interference with the static hand properties described by the original attributes while alleviating the computational overhead of a deeper network. Additionally, we enforce consistency between geometric and appearance (e.g., shadows align with deformations) through a lightweight attention mechanism. Second, we enhance the current densification strategy in 3DGS with a local-aware scheme by computing a local gradient score to dynamically adjust the Gaussian density in high-variation regions, improving finer detail preservation while maintaining efficiency in smoother areas. Third, we propose a pose-conditioned attribute regularization that encourages attribute consistency across similar poses by aligning Gaussian attributes with exponentially weighted moving averages (EMA) of historical memory, weighted by pose similarity. This maintains coherence while allowing pose-specific variations.

We conduct extensive experiments on InterHand2.6M, demonstrating that HandSplat significantly outperforms existing methods in both quantitative and qualitative evaluations. Our method achieves higher visual fidelity while maintaining fast rendering speeds suitable for real-time applications. The contributions of this paper are as follows:

1. We present HandSplat, a 3D Gaussian Splatting-based method that enhances hand modeling by incorporating learnable geometry and appearance embeddings, enabling finer non-rigid deformations while maintaining efficiency.
2. We introduce a pose-conditioned attribute regularization to enforce attribute coherence across similar poses and a local gradient-aware densification strategy to refine details in high-variation regions.
3. Extensive experiments on InterHand2.6M demonstrate that HandSplat outperforms existing methods both quantitatively and qualitatively while maintaining fast rendering speeds.

2. Related Work

2.1. Hand Avatar

The development of high-fidelity, animatable hand avatars has recently advanced significantly. A widely adopted method is explicit parametric mesh representation, which effectively captures hand geometry and texture through a set of parameters. The most widely used model is MANO [25], which serves as the foundation for numerous methods [5, 12, 14, 16, 23]. HTML [23] extends the MANO [25] model with a PCA-based appearance model, unifying geometry and texture. NIMBLE [16] improves this with anatomically accurate mesh models by incorporating bones, muscles, and physical-based textures. HARP [12] enhances realism with explicit albedo and normal UV maps. However, these methods are limited in capturing fine-grained details, often producing overly smooth surfaces. Increasing mesh resolution partially alleviates this but further introduces substantial computational and storage overhead.

Another research direction explores neural implicit representations for more realistic texture modeling. LISA [3] learns an implicit representation by predicting per-bone color and signed distance fields. HandAvatar [2] improves appearance modeling with albedo and illumination. HandNeRF [7] adapts NeRF with hand-specific deformation fields, and LiveHand [20] integrates a Hybrid structure by combining mesh with NeRF, reducing sampling requirements and accelerating inference. However, NeRF-based methods still have long training and inference time issues due to dense ray sampling and expensive MLP evaluations. Even with hybrid representations, they remain fundamentally constrained by NeRF’s implicit nature, where scene information is encoded as continuous functions rather than

discrete structures. This formulation makes NeRF difficult to enforce sharp boundaries or capture high-frequency textures, leading to challenges such as low resolution, over-smoothing, and color bias.

Recently, 3D Gaussian Splatting has achieved remarkable success in representing a 3D deformable hand by modeling geometry and appearance through continuous and differentiable Gaussian primitives [9, 11, 22, 27, 30, 32]. 3D-PSHR [11] incorporates albedo and shading into Gaussian representation. GaussianHand [30] refines hand reconstruction via blend shapes and residual pose correction. MANUS [22] focuses on hand-object interactions by estimating contact regions, and InterHandGS [9] models cross-subject interacting hands from single-image using a two-stage GS framework, with interaction modeling. Despite their success, these approaches still inherit static-scene 3DGS attributes and rely on skeletal motion for non-rigid estimation without explicitly capturing fine-grained geometric and photometric variations, limiting their ability to model non-rigid hand deformations. Additionally, none of these methods exploit the inherent consistency across similar poses. Regarding densification, existing methods apply per-point densification without considering local structures, resulting in suboptimal point distributions.

2.2. Gaussian-based Human Avatar

There is considerable literature exploring how to render a clothed human body [8, 10, 15, 21, 31, 33]. GauHuman [8], 3DGS-Avatar [24], and HUGS [15] focus on monocular video-based reconstruction, defining a canonical model and optimizing human Gaussians via SMPL parameters with the Linear Blend Skinning (LBS) transformations. While HiFi4G [10] emphasises the multi-view reconstruction by introducing a compact 4D Gaussian model with a dual-graph mechanism for spatial-temporal consistency. Though it preserves consistency, it requires video input with temporal ordering. In contrast, our approach addresses this differently by introducing pose similarity weighting, enabling consistency even with unordered frames. GPSGaussian [31] and MVSGaussian [17] focus on generalizable multi-view Gaussian models for high-quality human rendering. While these methods effectively model the human body, hands exhibit more complex deformations than the human body, featuring frequent self-occlusion and inter-finger contact, making direct transfer from body models ineffective.

3. Method

3.1. Preliminaries

3D Gaussian Splatting. 3D Gaussian Splatting represents a static scene using a set of 3D Gaussians \mathcal{G} , where each Gaussian \mathcal{G}_i is defined by its position \mathbf{x}_i and covariance ma-

trix Σ_i . The shape of Gaussian \mathcal{G}_i can be described as:

$$\mathcal{G}_i = e^{-\frac{1}{2}\mathbf{x}_i^T \Sigma_i^{-1} \mathbf{x}_i} \quad (1)$$

where Σ_i governs the spread and orientation of the Gaussian. To ensure valid matrices during optimization, the covariance matrix is decomposed into a rotation matrix \mathbf{D} and a scaling matrix \mathbf{S} , represented as $\Sigma = \mathbf{DSS}^T \mathbf{D}^T$.

To render 3D Gaussians, a depth-ordered set of N 3D Gaussians is projected from 3D world space to 2D image space using point-based α -blending. The final color of a pixel is computed as:

$$\mathbf{C} = \sum_{i \in N} \mathbf{c}_i \alpha_i \prod_{j=1}^{i-1} (1 - \alpha_j), \quad (2)$$

where N refers to the number of Gaussian points, \mathbf{c}_i represents the color of the i^{th} 3D Gaussian, and α_i is its opacity. The 3D Gaussians attributes are optimized to minimize pixel reconstruction loss. This process employs an adaptive density control policy including cloning, splitting, and pruning operations to dynamically adjust the representation.

3.2. Baseline: MANO-Driven Gaussian Dynamics

We model 3D hand shapes and textures in a canonical space, where each vertex of the MANO model is initialized as a 3D Gaussian and driven by MANO parameters.

LBS Weight and Pose Refinement. Inspired by [8] for human avatars, we refine both the Linear Blend Skinning (LBS) weights and MANO pose parameters. For the LBS weights, each Gaussian is initially assigned the LBS weights of its nearest MANO vertex, denoted as ω^{mano} . A shallow MLP Φ_{lbs} then predicts correction offsets, yielding the final weight ω_{lbs} :

$$\omega_{\text{lbs}} = \sigma \left(e^{\log(\omega^{\text{mano}} + \epsilon)} + \Phi_{\text{lbs}}(\gamma(\mathbf{x}^c)) \right), \quad (3)$$

where σ represents the softmax activation function, γ refers to sinusoidal positional encoding, and $\epsilon = 10^{-8}$.

Similarly, we use a learnable MLP Φ_{pose} to correct the initial MANO pose:

$$\boldsymbol{\theta}' = \boldsymbol{\theta} \otimes \Phi_{\text{pose}}(\boldsymbol{\theta}) \quad (4)$$

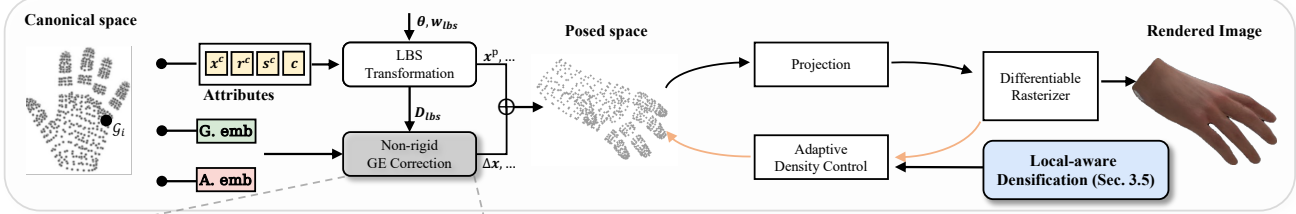
where \otimes refers to matrix multiplication and $\boldsymbol{\theta}$ represents a joint pose using quaternions.

LBS Transformation. With the corrected pose and LBS weights, we compute the LBS rotation matrix \mathbf{R}_i and translation vector \mathbf{T}_i for the i^{th} 3D Gaussian:

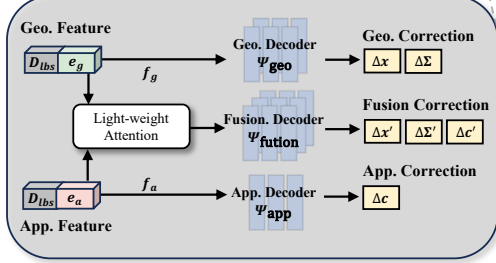
$$\{\mathbf{R}_i, \mathbf{T}_i\} = \sum_{k=1}^K \omega_{\text{lbs}} \{\mathbf{R}'_k(\mathbf{J}, \boldsymbol{\theta}'), \mathbf{T}'_k(\mathbf{J}, \boldsymbol{\theta}', \boldsymbol{\beta})\}. \quad (5)$$

where \mathbf{R}'_k and \mathbf{T}'_k denotes the k^{th} joint rotation matrix and translation vector, respectively. $\boldsymbol{\beta}$ represents the shape parameters in the MANO model, K is the number of hand

Baseline (Sec. 3.2)



Gaussian-Embedded Correction (Sec. 3.3)



Pose-Conditioned Attribute Regularization (Sec. 3.4)

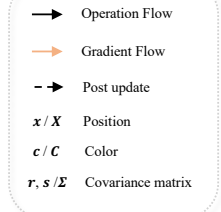
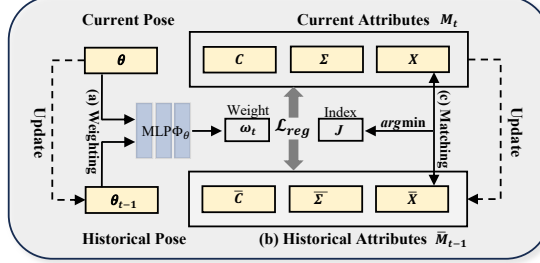


Figure 2. HandSplat Framework. For each 3D Gaussian \mathcal{G}_i in canonical space, HandSplat assigns two embedding attributes, e_g and e_a , to model non-rigid geometry and appearance features. The GE Correction module then predicts attribute corrections, which are applied to the attributes transformed by LBS to obtain posed hand Gaussians. These updated Gaussians are subsequently projected and rendered. Next, the Pose-Conditioned Attribute Regularization improves consistency across similar poses by comparing attributes of matched Gaussian pairs (c) in the current state M_t with historical memory \bar{M}_{t-1} (b), weighted by pose-conditioned factor ω_t (a). Finally, Local-Aware Densification refines Gaussian density by adapting to local geometric variations, preserving fine details.

joints in the MANO model, J refers to the Jacobian matrix approximating projective transformation from camera coordinate to ray coordinate. Then, the 3D position and covariance matrix of 3D Gaussian i is obtained as:

$$\mathbf{x}_i^p = \mathbf{R}_i \mathbf{x}_i^c + \mathbf{T}_i, \quad \Sigma_i^p = \mathbf{R}_i \Sigma_i^c \mathbf{R}_i^T, \quad (6)$$

where \mathbf{x}_i^p , Σ_i^p denote the position and covariance matrix in the posed space, while \mathbf{x}_i^c and Σ_i^c are their counterparts in the canonical space.

3.3. Gaussian-Embedded Correction

The rigid transformation provides only an approximate estimation and fails to capture subtle shape and visual variations. Previous works [11, 24, 27] have highlighted this limitation but found it challenging to address due to the simplistic structure and the static nature of the standard attributes.

To overcome these issues, inspired by [1], we introduce two implicit attributes for each Gaussian: geometry embedding $e_g \in \mathbb{R}^d$ and appearance embedding $e_a \in \mathbb{R}^d$. Unlike [1], which employs a single embedding for time-dependent deformations in dynamic scenes, our approach is specifically designed for hand Gaussian splatting and utilizes separate embeddings to independently model motion-related geometric and appearance variations. This representation enables more effective modeling of non-rigid motion while preserving inherent hand properties, thereby improving hand reconstruction quality. Additionally, we also introduce a lightweight attention mechanism to generate modulated embeddings, further enhancing the coherence between geometry and appearance.

These embeddings are optimized through the same differentiable rendering pipeline as standard 3DGS attributes and undergo identical densification and pruning operations, ensuring full compatibility with the original 3DGS framework while extending its representational capacity.

Specifically, for the i^{th} Gaussian point, we concatenate its geometry e_g and appearance e_a embeddings with the flattened LBS transformation matrix $\mathcal{D}_i = \mathbf{R}_i \mid \mathbf{T}_i$, where \mid denotes matrix concatenation. This constructs motion-aware geometry feature \mathbf{f}_{gi} and appearance feature \mathbf{f}_{ai} , which are then used to predict initial adjustments for other attributes:

$$\{\Delta \mathbf{x}_i, \Delta \Sigma_i\}, \Delta c_i = \Psi_{\text{geo}}(\mathbf{f}_{gi}), \Psi_{\text{app}}(\mathbf{f}_{ai}), \quad (7)$$

where Ψ_{geo} is a composite geometry decoder consisting of two shallow MLPs for predicting position and covariance variations, respectively. Ψ_{app} is an appearance decoder with a single shallow MLP for color variations prediction.

Adaptive Feature Fusion. While this separation embedding addresses motion-aware geometry and appearance features, localized coordination between geometry and appearance remains critical, for example, shadows near bent joints must align with deformations. To address this, we introduce a lightweight attention mechanism that learns adaptive blending weights for feature fusion.

Given geometry features \mathbf{f}_{gi} and appearance features \mathbf{f}_{ai} , the attention weights are computed as:

$$\mathbf{A}_{ga,i} = \sigma(\mathbf{W}(\mathbf{f}_{gi} \parallel \mathbf{f}_{ai})), \quad (8)$$

where $\mathbf{A}_{ga,i} \in \mathbb{R}^d$ modulates each dimension separately, and $\mathbf{W} \in \mathbb{R}^{d \times 2d}$ is a learnable weight matrix, \parallel denotes concatenation, and σ is the sigmoid activation function. The fused geometry feature is then computed as:

$$\tilde{\mathbf{f}}_{gi} = \mathbf{A}_{ga,i} \odot \mathbf{f}_{gi} + (1 - \mathbf{A}_{ga,i}) \odot \mathbf{f}_{ai}, \quad (9)$$

where \odot denotes element-wise multiplication. The fused appearance feature $\tilde{\mathbf{f}}_{ai}$ is computed in the same way by swapping \mathbf{f}_{gi} and \mathbf{f}_{ai} . Then, the fused adjustments are obtained as:

$$\Delta \mathbf{x}'_i, \Delta \Sigma'_i, \Delta c'_i = \Psi_{\text{fusion}}(\tilde{\mathbf{f}}_{gi} \parallel \tilde{\mathbf{f}}_{ai}), \quad (10)$$

where Ψ_{fusion} is a fusion decoder with three MLPs, each responsible for predicting position, covariance, and appearance variations, respectively.

Final Gaussian Update. The final Gaussian parameters in posed space are computed as:

$$\begin{aligned} \mathbf{x}_i &= \mathbf{x}_i^p + \Delta \mathbf{x}_i + \Delta \mathbf{x}'_i, & c_i &= c_i^p + \Delta c_i + \Delta c'_i, \\ \Sigma_i &= (\Delta \Sigma'_i \Delta \Sigma_i) \Sigma_i^p (\Delta \Sigma_i \Delta \Sigma'_i), \end{aligned} \quad (11)$$

where \mathbf{x}_i , Σ_i , and c_i are the i^{th} 3D Gaussian's final position, covariance, and color in the posed space, respectively.

3.4. Pose-Conditioned Attribute Regularization

Existing 3DGS-based hand methods treat each hand pose independently, ignoring the consistency of Gaussian attributes across similar poses. To address this, we introduce a pose-conditioned regularization that encourages similar poses to maintain consistent attribute values while also referencing historical attributes.

Specifically, at the t^{th} frame, we hold the current 3D Gaussian attribute set \mathbf{M}_t in posed space, and the current hand pose θ_t . Additionally, we maintain a historical attributes memory, denoted as $\bar{\mathbf{M}}_{t-1}$, which aggregates information from multiple past frames, and the previous hand pose θ_{t-1} , which provides a direct reference to the last frame. Here, $\mathbf{M} = \{\mathbf{X}, \Sigma, \mathbf{C}\}$ represents the position, covariance matrix, and color of all Gaussians.

This regularization loss is formulated through three synergistic components: pose-conditioned weighting, historical attributes memory and correspondence matching.

Pose-conditioned weighting. To encourage attribute consistency across similar poses, we define a regularization weight based on pose similarity between consecutive frames, assigning higher weights to more similar poses. We compute this weight by comparing the poses at t^{th} and $(t-1)^{\text{th}}$ frames:

$$\omega_t = \exp\left(-\frac{\|\Phi_\theta(\theta_t) - \Phi_\theta(\theta_{t-1})\|_2^2}{2\delta^2}\right) \quad (12)$$

where Φ_θ is a lightweight trainable MLP and δ is a trainable decay factor that controls the sensitivity of pose similarity. Both are optimized end-to-end.

Historical Attributes Memory. We maintain a historical attributes memory through exponential moving averages (EMA), which not only emphasises the attributes in the last frame but also preserves the past attributes. At the t^{th} frame, the loss uses the historical attributes from the previous frame, $\bar{\mathbf{M}}_{t-1}$, while the update for $\bar{\mathbf{M}}_t$ occurs after loss computation:

$$\bar{\mathbf{M}}_t = \rho \mathbf{M}_{t-1} + (1 - \rho) \bar{\mathbf{M}}_{t-1}, \quad (13)$$

Here, ρ controls the contribution of past frames to the buffer. For initialization, the first observation is set as $\bar{\mathbf{M}}_1 = \mathbf{M}_1$.

This formulation aggregates information from past frames, where the contribution of the k -th frame ($k < t$) decays as $\rho(1 - \rho^{t-k})$, ensuring that older, less-optimized frames have diminishing influence. The combined effect of pose-conditioned weighting and historical decay yields the final reference:

$$\bar{\mathbf{M}}_t \propto w_t \rho (1 - \rho^{t-k}) \mathbf{M}_k, \quad (14)$$

which helps reduce the influence of immature attributes.

Correspondence Matching. To establish correspondences between \mathbf{M}_t and $\bar{\mathbf{M}}_{t-1}$, we assign each Gaussian in \mathbf{M}_t to its nearest neighbor in $\bar{\mathbf{M}}_{t-1}$:

$$J = \text{argmin} \|\mathbf{X}_t - \bar{\mathbf{X}}_{t-1}\|_2^2, \quad (15)$$

where $J \in \mathbb{R}^{N \times 1}$ stores the index of the closest Gaussian in historical memory for each current Gaussian, N is the number of 3D Gaussians.

Attribute Regularization Loss. With the above three components, we formulate the regularization loss for the position attribute as:

$$\mathcal{L}_{\text{reg-x}} = \omega_t \sum_{i=1}^N \|\mathbf{x}_{t,i} - \bar{\mathbf{x}}_{(t-1),J(i)}\|_2^2, \quad (16)$$

where $\mathbf{x}_{t,i} \in \mathbf{X}_t$, $J(i)$ indexes the nearest historical Gaussian for the i -th Gaussian, and $\|\cdot\|_2$ denotes L2 norm. Similarly, we apply the same structure to covariance matrices and color, ensuring uniform regularization across all attributes. The total regularization loss is given by:

$$\mathcal{L}_{\text{reg}} = \lambda_x \mathcal{L}_{\text{reg-x}} + \lambda_\Sigma \mathcal{L}_{\text{reg-}\Sigma} + \lambda_c \mathcal{L}_{\text{reg-c}}, \quad (17)$$

where, λ_x , λ_Σ , and λ_c are weighting factors.

3.5. Local-aware Densification

Standard 3DGS densification is based on per-point gradients, which may overlook regions requiring collective refinement. We enhance this with a local-aware criterion, where a Gaussian is flagged for densification (clone or split) if its local neighborhood exhibits high aggregated view-space positional gradients.

For each Gaussian \mathcal{G}_i , its local neighborhood $\mathcal{N}(i)$ is defined using k-nearest neighbors (kNN). The influence ω_{ji} of

a neighbor \mathcal{G}_j on \mathcal{G}_i is given by:

$$\omega_{ji} = \frac{e^{-\eta d_{ji}}}{\sum_{k \in \mathcal{N}(i)} e^{-\eta d_{ki}}} \quad (18)$$

where d_{ji} is the distance between \mathcal{G}_j and \mathcal{G}_i , and η controls the weight decay with distance. A Gaussian is flagged for densification when the weighted sum of neighborhood gradients exceeds a threshold τ_{neigh} :

$$\sum_{j \in \mathcal{N}(i)} \omega_{ji} \nabla_j > \tau_{\text{neigh}} \quad (19)$$

where ∇_j is the gradient of \mathcal{G}_j . Flagged Gaussians are cloned or split following the original 3DGS strategy, with new Gaussians inheriting attributes from their parents.

3.6. Loss Function

Following other hand 3DGS-based methods [11, 22], we apply a standard RGB loss, mask loss, SSIM loss, and LPIPS loss to supervise the 3D model, defined as:

$$\mathcal{L}_{\text{base}} = \mathcal{L}_{\text{rgb}} + \lambda_1 \mathcal{L}_{\text{mask}} + \lambda_2 \mathcal{L}_{\text{SSIM}} + \lambda_3 \mathcal{L}_{\text{LPIPS}}, \quad (20)$$

where λ are loss weights. Empirically, we set $\lambda_1 = 0.1$, $\lambda_2 = \lambda_3 = 0.01$. Besides, to maintain the local smoothness of embedding, following [1], we also apply a smooth loss on the geometry embedding:

$$\mathcal{L}_{\text{emb}} = \frac{1}{kN} \sum_{i \in N} \sum_{j \in \text{KNN}_{i,k}} (w_{i,j} \| \mathbf{e}_{g_i} - \mathbf{e}_{g_j} \|_2), \quad (21)$$

where $w_{i,j} = \exp(-\lambda_w \| \mathbf{x}_j - \mathbf{x}_i \|_2^2)$ is the weighting factor. We set λ_w to 2000 and k to 20. The overall loss $\mathcal{L} = \mathcal{L}_{\text{base}} + \lambda_{\text{emb}} \mathcal{L}_{\text{emb}} + \lambda_{\text{reg}} \mathcal{L}_{\text{reg}}$, where λ are loss weights.

4. Experiments

Datasets and Metrics. We conduct experiments on the widely used InterHand2.6M [19] dataset, which provides large-scale multi-view sequences of diverse hand poses. To fairly assess our method, we select right-hand sequences from three subjects: test/Capture0, test/Capture1, and val/Capture0, focusing on ROM03, ROM04, and ROM07. Following LiveHand, we allocate the last 50 frames for testing and use the remaining frames for training, resulting in a split of approximately 93,000 (train) vs. 7,000 (test) frames. We evaluate PSNR, SSIM [28] and LPIPS [29] as metrics for the rendering results in full image. For the SSIM, we use VGG [26] with a window size of 11. We use FPS to compare the rendering speed across different systems.

Comparison Methods. To evaluate the performance of HandSplat, we conduct comprehensive comparisons with state-of-the-art NeRF-based and Gaussian Splatting-based methods, including HandAvatar [2], LiveHand [20] and

GauHuman [8]¹. All baseline results are generated using their publicly released code with default configurations to ensure fair comparison. For fairness, we only compare open-source methods. Other reported state-of-the-art methods, such as GaussianHand, JGHand, and 3D-PSHR, were not included in our comparison because they were not open-source at the time of submission, making it hard to guarantee fairness.

4.1. Quantitative Results

Tab. 1 summarizes the novel pose rendering results of LiveHand, GauHuman, HandAvatar, and our HandSplat across three subjects. Our method consistently outperforms all baselines in rendering quality, achieving the highest PSNR, SSIM, and lowest LPIPS across all test cases. Even though LiveHand [20] incorporates a speed-up method, it fails to maintain high rendering quality, particularly struggling with complex hand articulations, as indicated by its lower PSNR and SSIM scores. Although GauHuman [8] achieves the fastest rendering speed at 119 FPS, its rendering quality remains inferior, scoring 0.99 lower PSNR and 30% higher LPIPS on test/Capture1 compared to our method. This is also evident in qualitative comparisons, where blurry details, artifacts and inconsistencies are observed. Regarding training efficiency, HandAvatar [2] requires over 30 days to train on our dataset split under its original settings. To ensure a fair comparison, we adopt HandAvatar’s official dataset split instead. While HandAvatar achieves reasonable rendering quality, its training remains computationally expensive, taking over 8 days, and inference is extremely slow, requiring over 30 minutes for just 200 frames (0.10FPS). In contrast, our method achieves a 660× faster inference speed (66 FPS vs. 0.10 FPS), completing the same frames in just 5 seconds. Notably, our method achieves better performance when trained on sufficient and diverse poses, demonstrating its robustness and generalization capability.

4.2. Qualitative Results

Visual comparisons in Fig.3 show that HandSplat effectively captures high-frequency details, such as fingerprints, joint wrinkles, and subtle shading variations, while exhibiting fewer artifacts under challenging hand poses. As indicated by the red arrows, LiveHand suffers from blurring and over-smoothing, particularly in fine texture regions, which is caused by its implicit representation’s resolution limitations. This results in low-detail reconstructions, making fingernails and joint creases nearly imperceptible. Additionally, the hand color appears biased, contributing to relatively lower quantitative results. While GauHuman achieves faster rendering, the red-highlighted areas indicate

¹We modified the GauHuman framework by replacing the SMPL body model with the MANO hand model to specialize it for human hand.

Method	test/Capture0			test/Capture1			val/Capture0			FPS
	PSNR \uparrow	SSIM \uparrow	LPIPS \downarrow	PSNR \uparrow	SSIM \uparrow	LPIPS \downarrow	PSNR \uparrow	SSIM \uparrow	LPIPS \downarrow	
LiveHand	29.17	0.949	0.0528	26.85	0.776	0.0619	29.33	0.893	0.0606	69
GauHuman	32.29	0.958	0.0424	32.19	0.962	0.0445	31.64	0.954	0.0488	119
Ours	33.04	0.964	0.0338	33.18	0.968	0.0342	32.50	0.960	0.0391	66
HandAvatar*	29.86	0.948	0.0546	28.48	0.947	0.0569	29.87	0.946	0.0565	0.1
Ours*	31.75	0.954	0.0450	29.18	0.947	0.0547	31.11	0.949	0.0545	66

Table 1. **Quantitative comparison** of our method and baseline methods on the InterHand2.6M [19] dataset. Bold text denotes the best result for each metric. Our methods achieves the state-of-the-art PSNR, SSIM and LPIPS with real-time rendering. * To compare with HandAvatar, we adopt HandAvatar’s train-test split.

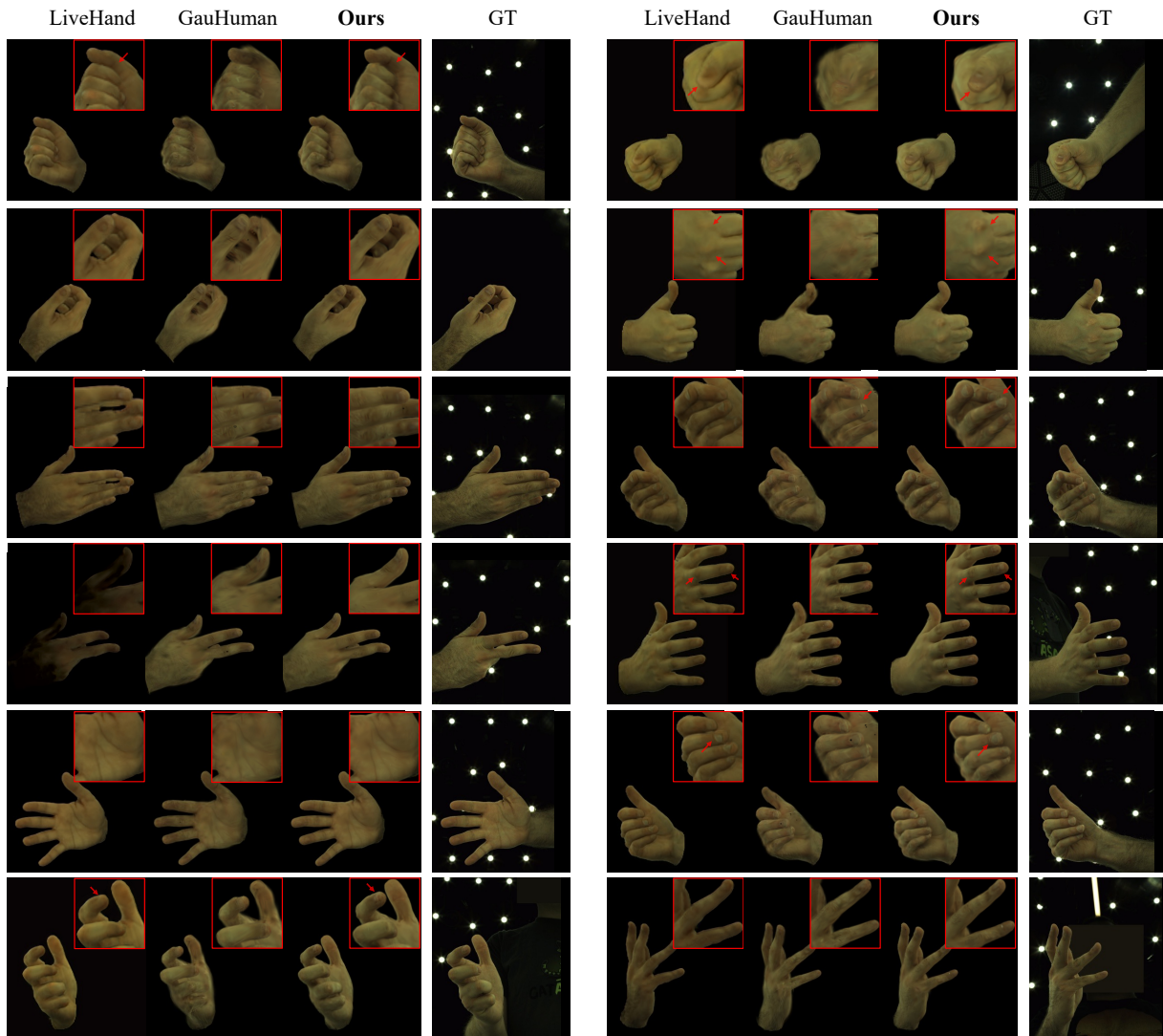


Figure 3. **Qualitative Comparison on InterHand2.6M [19]**. We present the novel pose animation results for three subjects using LiveHand [20], GauHuman [8], and our method. LiveHand produces over-smoothed, low-resolution renderings with noticeable color bias, while GauHuman introduces artifacts and fails to capture high-frequency details. In contrast, ours achieves high-quality reconstructions, effectively preserving fine geometric details (e.g., wrinkles, fingernails) and appearance variations (e.g., shadows, highlights), even on out-of-distribution poses.

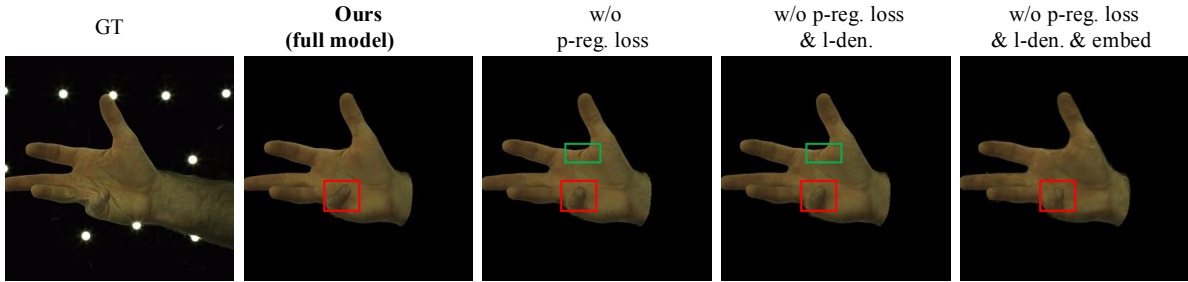


Figure 4. **Ablation Study** on the test/cap0 of Interhand2.6M dataset.

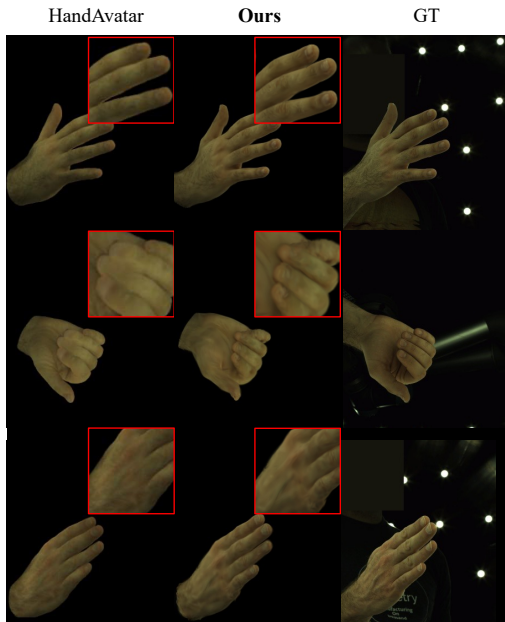


Figure 5. **Qualitative Comparison on InterHand2.6M [19] with HandAvatar’s dataset split.** HandAvatar produces over-smoothed results and falls short in modeling shading and lighting variations, leading to loss of details.

significant noise and artifacts, such as black spots in fine textures, causing loss of detail in skin creases. This results in unnatural surface textures, particularly in challenging hand poses like fist clenching or extreme finger bending, where it becomes difficult to distinguish clear finger boundaries and fingernails. Additionally, the reconstructed hand pose is sometimes inaccurate under extreme articulations as shown in the third line and second column. The red-boxed regions in Fig. 5 for HandAvatar’s reveal under-reconstruction in high-frequency areas, leading to missing wrinkles and poor shading consistency. Additionally, HandAvatar struggles to capture realistic shadow effects, resulting in inconsistent illumination among fingers.

As seen in the red-boxed regions in Fig. 3 and Fig. 5, our method faithfully reconstructs high-frequency details, ensuring sharp textures and realistic shading, even under complex articulations. The red arrows indicate that our approach maintains shading continuity, accurately preserving

GEC	PCAR	LAD	PSNR \uparrow	SSIM \uparrow	LPIPS \downarrow
\times	\times	\times	32.13	0.958	0.0427
\checkmark	\times	\times	32.85	0.963	0.0340
\checkmark	\checkmark	\times	32.99	0.964	0.0342
\checkmark	\checkmark	\checkmark	33.04	0.964	0.0338

Table 2. The proposed model achieves the highest PSNR and SSIM and the lowest LPIPS, demonstrating the effectiveness of all components.

shadow consistency across fingers and palm regions. Furthermore, HandSplat generalizes robustly to unseen poses, retaining structural integrity and fine-grained details even in extreme deformations.

4.3. Ablation Study

We study the effect of various components of our method on the InterHand2.6M dataset of subject “test/Capture0”, including Gaussian-Embedded Correction (GEC), Pose-Conditioned Attribute Regularization (PCAR), and Local-aware Densification (LAD).

The quantitative results in Tab. 2 show that each component contributes to the overall performance, and all proposed techniques are required to reach the optimal results. Specifically, introducing DEMAR alone already brings a +0.72 dB PSNR gain (32.85 vs. 32.13) and a 20% LPIPS reduction (0.0340 vs. 0.0427), highlighting the importance of fine-grained motion-aware refinement. Adding PCAS further enhances consistency across frames, improving PSNR to 32.99. Finally, LGGD refines high-detail regions, reaching the best PSNR of 33.04 and the lowest LPIPS of 0.0338.

We further present a qualitative comparison on out-of-distribution poses in Fig. 4, showing that removing PCAR reduces fine details, such as fingernails. Excluding LAD results in the loss of fine details, particularly in wrinkles (green box) and fingernails (red box). Without GEC, high-frequency geometric and appearance details degrade, introducing more artifacts and reducing overall visual fidelity. These findings confirm that each component is essential for improving generalization to novel poses.

5. Conclusion

This paper proposes HandSplat, a novel Gaussian Splatting-based framework for high-fidelity and stable hand rendering. Our method enhances non-rigid motion modeling with learnable geometry and appearance embeddings, improves temporal consistency through pose-aware attribute regularization, and refines detail preservation with local-aware densification. Extensive experiments on InterHand2.6M show that HandSplat surpasses existing methods in fidelity, stability, and efficiency, demonstrating a significant advancement in hand reconstruction.

References

- [1] Jeongmin Bae, Seoha Kim, Youngsik Yun, Hahyun Lee, Gun Bang, and Youngjung Uh. Per-gaussian embedding-based deformation for deformable 3D gaussian splatting. In *European Conference on Computer Vision*, pages 321–335. Springer, 2024. 4, 6
- [2] Xingyu Chen, Baoyuan Wang, and Heung-Yeung Shum. Hand Avatar: Free-pose hand animation and rendering from monocular video. In *Proceedings of the IEEE/CVF Conference on Computer Vision and Pattern Recognition*, pages 8683–8693, 2023. 1, 2, 6
- [3] Enric Corona, Tomas Hodan, Minh Vo, Francesc Moreno-Noguer, Chris Sweeney, Richard Newcombe, and Lingni Ma. Lisa: Learning implicit shape and appearance of hands. In *Proceedings of the IEEE/CVF Conference on Computer Vision and Pattern Recognition*, pages 20533–20543, 2022. 2
- [4] Guy Gafni, Justus Thies, Michael Zollhofer, and Matthias Nießner. Dynamic neural radiance fields for monocular 4D facial avatar reconstruction. In *Proceedings of the IEEE/CVF Conference on Computer Vision and Pattern Recognition*, pages 8649–8658, 2021. 1
- [5] Qijun Gan, Wentong Li, Jinwei Ren, and Jianke Zhu. Fine-grained multi-view hand reconstruction using inverse rendering. In *Proceedings of the AAAI Conference on Artificial Intelligence*, pages 1779–1787, 2024. 2
- [6] Xiangjun Gao, Jiaolong Yang, Jongyoo Kim, Sida Peng, Zicheng Liu, and Xin Tong. MPS-NeRF: Generalizable 3D human rendering from multiview images. *IEEE Transactions on Pattern Analysis and Machine Intelligence*, 2022. 1
- [7] Zhiyang Guo, Wengang Zhou, Min Wang, Li Li, and Houqiang Li. Handnerf: Neural radiance fields for animatable interacting hands. In *Proceedings of the IEEE/CVF Conference on Computer Vision and Pattern Recognition*, pages 21078–21087, 2023. 1, 2
- [8] Shoukang Hu, Tao Hu, and Ziwei Liu. GauHuman: Articulated gaussian splatting from monocular human videos. In *Proceedings of the IEEE/CVF Conference on Computer Vision and Pattern Recognition*, pages 20418–20431, 2024. 1, 2, 3, 6, 7
- [9] Xuan Huang, Hanhui Li, Wanquan Liu, Xiaodan Liang, Yiqiang Yan, Yuhao Cheng, and Chenqiang Gao. Learning interaction-aware 3D gaussian splatting for one-shot hand avatars. *Advances in Neural Information Processing Systems*, 37:14127–14147, 2025. 3
- [10] Yuheng Jiang, Zhehao Shen, Penghao Wang, Zhuo Su, Yu Hong, Yingliang Zhang, Jingyi Yu, and Lan Xu. HiFi4G: High-fidelity human performance rendering via compact gaussian splatting. In *Proceedings of the IEEE/CVF Conference on Computer Vision and Pattern Recognition*, pages 19734–19745, 2024. 3
- [11] Zheheng Jiang, Hossein Rahmani, Sue Black, and Bryan Williams. 3D points splatting for real-time dynamic hand reconstruction. *Pattern Recognition*, page 111426, 2025. 1, 2, 3, 4, 6
- [12] Korrawe Karunratanakul, Sergey Prokudin, Otmar Hilliges, and Siyu Tang. HARP: Personalized hand reconstruction from a monocular rgb video. In *Proceedings of the IEEE/CVF Conference on Computer Vision and Pattern Recognition*, pages 12802–12813, 2023. 2
- [13] Bernhard Kerbl, Georgios Kopanas, Thomas Leimkühler, and George Drettakis. 3D gaussian splatting for real-time radiance field rendering. *ACM Transactions on Graphics*, 42(4), 2023. 1, 2
- [14] Minje Kim and Tae-Kyun Kim. BiTT: Bi-directional texture reconstruction of interacting two hands from a single image. In *Proceedings of the IEEE/CVF Conference on Computer Vision and Pattern Recognition*, pages 10726–10735, 2024. 2
- [15] Muhammed Kocabas, Jen-Hao Rick Chang, James Gabriel, Oncel Tuzel, and Anurag Ranjan. HUGS: Human gaussian splats. In *Proceedings of the IEEE/CVF Conference on Computer Vision and Pattern Recognition*, pages 505–515, 2024. 2, 3
- [16] Yuwei Li, Longwen Zhang, Zesong Qiu, Yingwenqi Jiang, Nianyi Li, Yuexin Ma, Yuyao Zhang, Lan Xu, and Jingyi Yu. NIMBLE: a non-rigid hand model with bones and muscles. *ACM Transactions on Graphics*, 41(4):1–16, 2022. 2
- [17] Tianqi Liu, Guangcong Wang, Shoukang Hu, Liao Shen, Xinyi Ye, Yuhang Zang, Zhiguo Cao, Wei Li, and Ziwei Liu. MVSGaussian: Fast generalizable gaussian splatting reconstruction from multi-view stereo. In *European Conference on Computer Vision*, pages 37–53. Springer, 2024. 3
- [18] Ben Mildenhall, Pratul P Srinivasan, Matthew Tancik, Jonathan T Barron, Ravi Ramamoorthi, and Ren Ng. Nerf: Representing scenes as neural radiance fields for view synthesis. *Communications of the ACM*, 65(1):99–106, 2021. 1
- [19] Gyeongsik Moon, Shoou-I Yu, He Wen, Takaaki Shiratori, and Kyoung Mu Lee. InterHand2.6M: A dataset and baseline for 3D interacting hand pose estimation from a single RGB image. In *European Conference on Computer Vision*, pages 548–564. Springer, 2020. 6, 7, 8
- [20] Akshay Mundra, Jiayi Wang, Marc Habermann, Christian Theobalt, Mohamed Elgharib, et al. Livehand: Real-time and photorealistic neural hand rendering. In *Proceedings of the IEEE/CVF International Conference on Computer Vision*, pages 18035–18045, 2023. 1, 2, 6, 7
- [21] Haokai Pang, Heming Zhu, Adam Kortylewski, Christian Theobalt, and Marc Habermann. ASH: Animatable gaussian

- splats for efficient and photoreal human rendering. In *Proceedings of the IEEE/CVF Conference on Computer Vision and Pattern Recognition*, pages 1165–1175, 2024. 3
- [22] Chandradeep Pokhariya, Ishaan Nikhil Shah, Angela Xing, Zekun Li, Kefan Chen, Avinash Sharma, and Srinath Sridhar. MANUS: Markerless grasp capture using articulated 3D gaussians. In *Proceedings of the IEEE/CVF Conference on Computer Vision and Pattern Recognition*, pages 2197–2208, 2024. 1, 2, 3, 6
- [23] Neng Qian, Jiayi Wang, Franziska Mueller, Florian Bernard, Vladislav Golyanik, and Christian Theobalt. HTML: A parametric hand texture model for 3D hand reconstruction and personalization. In *European Conference on Computer Vision*, pages 54–71. Springer, 2020. 2
- [24] Zhiyin Qian, Shaofei Wang, Marko Mihajlovic, Andreas Geiger, and Siyu Tang. 3DGS-Avatar: Animatable avatars via deformable 3D gaussian splatting. In *Proceedings of the IEEE/CVF Conference on Computer Vision and Pattern Recognition*, pages 5020–5030, 2024. 1, 2, 3, 4
- [25] Javier Romero, Dimitrios Tzionas, and Michael J. Black. Embodied hands: modeling and capturing hands and bodies together. *ACM Transactions on Graphics*, 36(6), 2017. 2
- [26] Karen Simonyan and Andrew Zisserman. Very deep convolutional networks for large-scale image recognition. In *International Conference on Learning Representations*, 2015. 6
- [27] Zhoutao Sun, Xukun Shen, Yong Hu, Yuyou Zhong, and Xueyang Zhou. JGHand: Joint-driven animatable hand avatar via 3D gaussian splatting. *arXiv preprint arXiv:2501.19088*, 2025. 1, 2, 3, 4
- [28] Zhou Wang, Alan C Bovik, Hamid R Sheikh, and Eero P Simoncelli. Image quality assessment: from error visibility to structural similarity. *IEEE transactions on image processing*, 13(4):600–612, 2004. 6
- [29] Richard Zhang, Phillip Isola, Alexei A Efros, Eli Shechtman, and Oliver Wang. The unreasonable effectiveness of deep features as a perceptual metric. In *Proceedings of the IEEE/CVF Conference on Computer Vision and Pattern Recognition*, pages 586–595, 2018. 6
- [30] Lizhi Zhao, Xuequan Lu, Runze Fan, Sio Kei Im, and Lili Wang. Gaussianhand: Real-time 3D gaussian rendering for hand avatar animation. *IEEE Transactions on Visualization and Computer Graphics*, 2024. 1, 2, 3
- [31] Shunyuan Zheng, Boyao Zhou, Ruizhi Shao, Boning Liu, Shengping Zhang, Liqiang Nie, and Yebin Liu. GPS-Gaussian: Generalizable pixel-wise 3D gaussian splatting for real-time human novel view synthesis. In *Proceedings of the IEEE/CVF Conference on Computer Vision and Pattern Recognition*, pages 19680–19690, 2024. 3
- [32] Xiaozheng Zheng, Chao Wen, Zhuo Su, Zeran Xu, Zhaohu Li, Yang Zhao, and Zhou Xue. OHTA: One-shot hand avatar via data-driven implicit priors. In *Proceedings of the IEEE/CVF Conference on Computer Vision and Pattern Recognition*, pages 799–810, 2024. 3
- [33] Wojciech Zielonka, Timur Bagautdinov, Shunsuke Saito, Michael Zollhöfer, Justus Thies, and Javier Romero. Drivable 3D gaussian avatars. *arXiv preprint arXiv:2311.08581*, 2023. 3